Electrochimica Acta 313 (2019) 79–90

Contents lists available at ScienceDirect

Electrochimica Acta

journal homepage: www.elsevier.com/locate/electacta

Durable soft neural micro-electrode coating by an electrochemical synthesis of PEDOT:PSS / graphene oxide composites

Seunghyeon Lee [a, 1], Taesik Eom [a, 1], Min-Kyoung Kim [b, 1], Su-Geun Yang [b, **], Bong Sup Shim [a, *]

[a] Department of Chemical Engineering, Inha University, 100 Inharo, Michuholgu, Incheon, 22212, Republic of Korea
[b] Department of New Drug Development, Inha University College of Medicine., 366 Seohaedaero, Junggu, Incheon, 22332, Republic of Korea

ARTICLE INFO

Article history:
Received 24 November 2018
Received in revised form
26 February 2019
Accepted 15 April 2019
Available online 22 April 2019

Keywords:
Bioorganic electronics
Neural interface
Conducting polymers
PEDOT:PSS
Graphene oxides
Carbon composites
Neural micro-electrodes

ABSTRACT

The biocompatible neural interface has been one of the most difficult challenges in developing implantable active neural prostheses for more than a decade. Either in recording neural signals, which delivers intelligent signals to operate active prostheses or in stimulating living tissues, which aids sensing organ deficits, neural electrodes play central roles in relaying information between biotic tissues and abiotic electronics. Until now no single material can possess all the ideal physicochemical properties of chronically implantable neural electrodes although organic conducting polymers have demonstrated the most promising functional integration with neural tissues. Here, we have successfully constructed poly(3,4-ethylene dioxythiophene):poly(styrene sulfonate) (PEDOT:PSS)/graphene oxides (GOs) hybrid composites by electrochemical deposition on a gold micro-electrode. By changing the compositions and the redox states of GOs, the composites showed varied electrochemical performances as implantable neural electrodes, which have been further analyzed by Raman spectroscopy and scanning electron microscopy (SEM), and PC12 neural cellular attachment tests. Our experimental results indicated that both PEDOT:PSS/GOs and PEDOT:PSS/reduced graphene oxides (rGOs) were significantly better than PEDOT:PSS in electrochemical performances, mechanical softness, as well as favorable protein expressions of modulating PC12 neural cells. Therefore, our PEDOT:PSS/rGO composites can be used to further improve the PEDOT in the applications of an implantable electrode, biosensors, drug delivery carriers, and neural interfaces.

1. Introduction

Advances in modern electronic and robotic technologies have changed not just our daily life but also neural prosthetic devices. Human intention can be delivered as commanding signals to operate electronic computers or prosthetic robots through the so-called 'brain-machine interfaces' [1,2], 'body-machine interfaces', or 'peripheral nerve interfaces (PNIs)' [3]. Neurologic deficits, including Parkinson's disease [4], Lou Gehrig's disease, epilepsy [5], chronic pain [6,7], and depression [8], can also be treated by therapeutic neuro-stimulation. Electroceuticals will also be used to provide effective medical treatments to restore body function or regain health by intercepting an autonomous nervous system [9]. All these bionics require implantable neural electrodes, whose ideal qualities require seamless integration of both abiotic functionality and biotic cellular interactions. Because abiotic sides build electrical circuits, their desirable material properties are not limited to high electrical conductivity and mechanical integrity, but also include high signal-to-noise transduction and delicately tunable performances [10]. Biotic tissues, however, require them to have ionic conductivity, softness, conformability to complex extracellular structures, physiological stability, as well as facile relays of multi-cellular inter-communication. Thus, no single material can bridge seemingly contradictory property gaps between implantable electrode devices and biotic tissues.

Conventional materials for these neural electrode applications are dominantly rigid noble metals with Young's modulus of tens to hundreds GPa such as gold, platinum, and iridium, on flexible

* Corresponding author.
** Corresponding author.
E-mail addresses: sugeun.yang@inha.ac.kr (S.-G. Yang), bshim@inha.ac.kr (B.S. Shim).
[1] These authors contributed equally.

https://doi.org/10.1016/j.electacta.2019.04.099
0013-4686/

matrices. They are too rigid to be compatible with nerve tissues, such as brain which has few kPa of Young's modulus [11]. When neuronal cells are electrically stimulated, biphasic current pulses are used through these electrochemical working electrodes at the proximal interfaces of the cells. Thus, the electrochemical performances of the electrode determine the efficacies of safely stimulating or sensitively recording neural signals at the neural interfaces. Furthermore, pseudocapacitive charge transports rather than faradaic charge injections are preferably designed to trigger only action potentials through ion channels on cellular membranes, without causing potentially toxic side reactions, splitting water, or corroding metallic ions from the surfaces of the electrode. For this purpose, surface roughening on the metallic electrodes could be employed to increase charge storage capacities. However, this roughening generally does not prevent metal corrosion at all [12]. Even small amounts of dissolved metal ions are critical to cause not only neurotoxicity but also inflammatory reactions at the interface. Thus, it is also desirable to cover up the metallic exposures without causing impedance elevations, overshooting potentials, and losing mobile charge storage capacities[10].

Advanced electronic materials including carbon nanomaterials [13] and conducting polymers have been demonstrated to improve cytocompatibility as well as essential electrochemical functionalities. Poly(thiophenes), particularly poly(3,4-ethylene dioxythiophene) (PEDOT) is one of the most promising soft conducting polymers(~2.7 GPa) [14–16] in the applications of organic and flexible bioelectronics because of its unique chemical stability [17]. While conventional polymers have confined σ-bonded electrons in the sp^3 hybrid structures, PEDOT has delocalized charge carriers along the sp^2 hybrid orbitals of π-conjugated backbone structures. Two most common ways to prepare PEDOT materials are oxidative chemical and electrochemical polymerizations by adding desired doping materials. For the chemical method, two EDOT precursors are directly oxidized and integrated together. This process continues by strong oxidizing agents such as $FeCl_3$, Fe $(OTS)_3$ or $AgNO_3$. For the electrochemical way, the EDOT monomer is spatially oxidized by injected charges through the electrode. The EDOT oligomer then grows gradually into a blue colored polymer. Simultaneously, the PEDOTs are densely deposited on the electrode by hydrophobic interactions from an aqueous solution. These electrochemically prepared PEDOTs are intrinsically nanoporous to diffuse electrical charges along with the deposited layer effectively as well as to facilitate ionic charge transports through the polymeric volume. Furthermore, these PEDOT materials have demonstrated unique biocompatible performances, particularly when interfacing with biotic tissues. PEDOT could be directly synthesized in *in situ* biotic environments with living neural cells [18], through living tissues [19], and even in rat cortex [20]. PEDOT nanotubes have also been proved to be useful in reducing mechanical stiffness of metallic electrodes without losing electrochemical charge transductions [21]. Biocompatible doping materials of PEDOT like hyaluronic acid (HA) and heparin [22,23] as well as $LiClO_4$, PSS, and *p*-toluenesulfonic acid (PTS), could be used to modulate electrochemical and biocompatible properties in order to improve the device performances as neural interfaces.

Although these PEDOT materials have become essential in the neural interfaces, relatively poor electrochemical durability has remained as the challenging limitation to expand the chronically implantable applications of PEDOT [24,25]. As ionic and electrical charges are released from or headed into the PEDOT by repeated biphasic stimulations, the molecular structures of PEDOT are mechanically swelling, contracting and thus, breaking their conjugated backbones as well as concurrent doping/de-doping processes [14]. While polymeric dopants such as PSS could reinforce the structures moderately by molecular entanglements into PEDOT, electrochemical durability is still needed to be improved to be used as chronic implants. One approach to improve the electrochemical durability of soft conducting polymers is to build composites with carbon nanomaterials such as graphene and carbon nanotube (CNT) [26]. These carbon composites could improve electrochemical performances of the conducting polymers without altering chemical stability. Thus, the composite methodology has been used in the wide ranges of biomedical applications such as biosensors [27–35], drug delivery system [36,37], scaffolds for regeneration [38–43] and electrodes for bio-interfaces [44–50].

For neural interface applications, Cui group compared long-term neural recording performances of PEDOT:PSS and PEDOT/CNTs which were electrodeposited on the Au electrode [51]. The chronic recording performances were evaluated in the visual cortex of mice. The performances of PEDOT/CNTs significantly outperformed PEDOT:PSS after 7–8 weeks of implantation. They also tried to coat the PEDOT/CNT composites with an anti-inflammatory drug, dexamethasone, on the surface of Pt [52,53]. The results showed not only lowering the impedance values from bare Pt, but also significantly reducing neuronal deaths or damages *in vitro* and *in vivo*. Guo et al., reported the PEDOT:PSS/rGO microfibers for self-powered stimulation to enhance neural differentiation [39]. The microfibers, fabricated by a modified capillary hydrothermal method, were used for stimulation of mesenchymal stem cells to differentiate into a neural lineage.

In this experiment, we have successfully deposited the PEDOT:PSS/GO composites on Au micro-electrodes with different redox levels of GOs. The PEDOT:PSS/GO composites showed much-improved charge storage capacity (CSC) as well as electrochemical durability compared to PEDOT:PSS. Furthermore, redox state of GOs were quite effective parameters to freely tune the electrochemical properties of the PEDOT:PSS/GO composites. Surprisingly, our PEDOT:PSS/GO composites are softer and mechanically more durable than PEDOT:PSS itself at the same time. From our *in vitro* PC12 neural cell tests, the PEDOT:PSS/GO was not just cytocompatible but also able to modulate gene expression of specific proteins such as GAP-43, regulating axonal regeneration, and synapsin, enhancing cellular communications. Thus, our findings on PEDOT:PSS/GO composite coatings on Au micro-electrodes suggest that electrical performances, as well as cellular behaviors of neural interfaces, are easily tuned by compositions as well as redox state of GOs.

2. Experiment

2.1. Materials

Graphite (17046-02, 75–100 μm) was purchased at KANTO Chemical in Japan. Potassium permanganate ($KMnO_4$, 99.0%), sulfuric acid (H_2SO_4, 98.0%, 7683-4100), hydrochloric acid (HCl, 35.0–37.0%, 4090–4100) and hydrogen peroxide (H_2O_2, 30.0%, 4104–4405) were purchased at DAEJUNG in Korea. Sodium nitrate ($NaNO_3$, 99.0% 1475) was purchased at DUKSAN pure chemicals in Korea. Polystyrene sulfonate (PSS, Mw ~1,000,000, 434574), 3,4-ethylene dioxythiophene (EDOT, 97.0%, 483028) and phosphate-buffered saline (PBS, P4417) were purchased at Sigma-Aldrich in USA. Gold wire (0.1 mm diameter, 99.95%, 14727) was purchased at Alfa Aesar in USA. Epoxy resin (145–10025) and hardener (145–10030) was purchased at Allied High Tech Products Inc. The PC12 cells were purchased at Korean Cell Line Bank in Korea. Roswell Park Memorial Institute (RPMI) 1640 Medium and 100 × Antibiotics penicillin/streptomycin were obtained from Thermo Fisher Scientific (Waltham, MA, USA). Fetal bovine serum (FBS) was obtained from Hyclone (Pittsburgh, PA, USA). Cell Counting Kit-8 (CCK-8) was purchased from Dojindo Molecular Technologies, Inc

(Rockville, MD, USA).

2.2. Synthesis of graphene oxide

Graphene oxide was synthesized through the oxidization of graphite powder according to the modified Hummers method (Fig. 1(a)) [54]. 0.1 g of graphite, 5 ml of 98% sulfuric acid and 0.1 g of sodium nitrate were stirred under ice bath condition for intercalation of oxygen molecules to the graphite. After 10 min, the temperature of the beaker was set to 50 °C, and 0.05 g, 0.15 g and 0.25 g of potassium permanganate were slowly added. After 15 min, 25 ml of DI water for dilution, 3 ml of hydrogen peroxide for removing remaining salts were added. The pH level is adjusted to 10–11 using a sodium hydroxide solution to terminate the reaction. The solution was filtrated with enough amount of DI water. Cake from the filtration was dispersed to 50 ml of DI water with stirring. And graphene oxide pellet was collected through the centrifugation of dispersed solutions. The pellet was dispersed with 10 mg of PSS in 50 ml of DI water by using the bath sonication for overnight.

2.3. Reduction of graphene oxide

Hydrochloric acid was added to the graphene oxide solution to adjust the concentration to 1 M. An enough aluminum foil was immersed to the solution for 15 min. The reduced graphene oxide was precipitated to the bottom of the conical tube.

2.4. Preparation of EDOT/PSS/GO and EDOT/PSS/rGO solution

EDOT was dispersed in deionized water and GO and rGO solution at 0.02 M (2.21 μl/ml) with PSS at a weight ratio of 1:1. For good dispersion of EDOT, that solution was stirred vigorously.

2.5. Preparation of gold wire electrode

For electrochemical deposition of PEDOT:PSS and PEDOT:PSS/GO composites on the gold wire, the gold wire was sealed by epoxy. The epoxy resin and hardener were mixed at a ratio of 10:3. The mixture was poured into a petri dish and the pipette tip was cut at both ends and placed there. After curing in 50 °C oven at 2 h, the gold wire was put inside of pipette tip and filled with the epoxy mixture. That was cured at 50 °C oven for 2 h. Before the electrochemical deposition, all the electrodes were cut and polished by the sandpaper, CW-1200. The control bare gold electrode was also polished by the exact same process before characterization.

2.6. Electrochemical deposition and characterization of PEDOT:PSS, PEDOT:PSS/GO and PEDOT:PSS/rGO

The Gamry Reference600 Potentiostat (Gamry, USA) and the Gamry EIS300 Electrochemical Impedance Spectroscopy (EIS) Software, and the AutoLab PGSTAT204 Potentiostat and NOVA advanced software were used for both electrodeposition and all electrochemical characterization. EDOT monomers were polymerized through a chronopotentiometry method on the epoxy sealed gold electrode and ITO coated glass at 5 μA for 3 min and 2 V for 15 min respectively (see Fig. 1(b)). The counter electrode and the reference electrode were Pt plate and Ag/AgCl electrode respectively. After the deposition, 5 samples of each electrode were analyzed through EIS (1–100,000 Hz at 1 μA), symmetric bi-phasic stimulation (BPS), cyclic voltammetry (CV, −0.6–0.8 V, 50 mV/s, 3 cycles) and durability test (−1.0–1.0 V, 200 mV/s, 500 cycles). The BPS was performed to find charge injection limit (CIL) with the variable current for 500 μs and 200 μs of pulse and phase width, respectively. The morphology analysis was characterized by SEM (SU8010, Hitachi, Japan) after coating with Pt by using Sputter Coater (Q150T, Quorum Technologies Ltd, United Kingdom). The combination system of an Element Silicon Drift Detector (SDD) with the APEX™ software by AMETEK, Inc. was used for element energy dispersive spectroscopy (EDS). The Young's modulus was measured by nanoindentation system (G200, KLA, USA). The mechanical loads were collected in the depth range from 0 to 40–100 nm, and the average Young's modulus was calculated from the six of indentation results in the depth range of 20–30 nm. The LabRam GR UV/Vis/NIR (Horiba, Japan) was used to record Raman spectra.

2.7. Cell viability test

In vitro cytotoxicity of electrodes was determined in PC12 cells by the Cell Counting Kit-8 (CCK-8) assay. PC12 cells were incubated in RPMI medium containing 5% heat-inactivated FBS and 1% penicillin/streptomycin at 37 °C in 5% CO_2 humidified atmosphere. Each

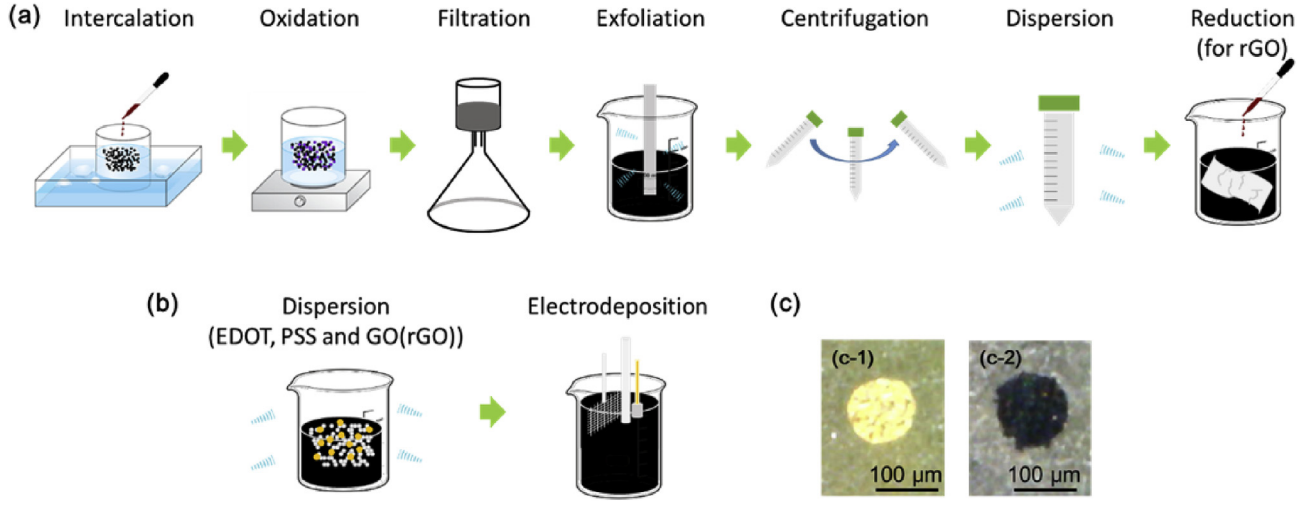

Fig. 1. Schematic of the process for (a) synthesis of GO and rGO (b) synthesis of PEDOT:PSS/GO composites. (c) Optical images of (c-1) bare gold electrode and (c-2) PEDOT:PSS/GO composite coated electrode. (For interpretation of the references to color in this figure legend, the reader is referred to the Web version of this article.)

electrode was sterilized by 70% ethanol solution for 1 h and exposed to UV for further sterilization. Each electrode was air-dried for one day and seeded with 10^5 cells/ml in a 24 well plate. After 72 h incubation, cells were trypsinized and collected by centrifugation with 1500 rpm for 10 min. After removing the supernatant, the pellet was collected with 350 μl cell media. 10 μl of CCK8 assay was added to 96 well plates containing 100 μl cell media and incubated for 2 h to produce formazan crystals. The absorbance of each well was measured using 420 nm wavelength with a microplate reader. The absorbance of the cells cultured without electrode was used as a control and its absorbance was as the reference value for calculating 100% cellular viability.

2.8. PC12 neuronal differentiation

The 2×10^3 cells were seeded on a 24 well plate with each sample. 24 h after, the medium was replaced with serum-free media supplemented with 50 ng/ml human recombinant NGF (Rockhill, NJ, USA). The cells were incubated for 7 days.

2.9. Total RNA isolation and quantitative real-time PCR (qPCR)

Total RNA was isolated from treated cells using the TRIzol reagent (Invitrogen, Waltham, MA, USA) according to the manufacturer's instructions. First strand cDNA was generated using a Tetro cDNA synthesis kit (Bioline Inc, UK). The target genes, relevant sense and antisense primers (Table 1) were measured as described previously [55]. These experiments were repeated for three times.

3. Results and discussions

3.1. Production of GO and rGO

The Raman spectra, shown in Fig. 2, were used to qualitative analyze GO and rGO which were produced by the modified Hummers method and chemical reduction, respectively. In the graph, the numbers next to the GO and the rGO means the amount of potassium permanganate, which controls the degree of oxidation. GO(05) were synthesized with 0.05 g of potassium permanganate, GO(15) with 0.15 g, GO(25) with 0.25 g of that, respectively. The rGO is the reduced form of these GOs by oxidation of Al foil. As in the typical graphene analysis, G band at ~1580 cm^{-1}, D band at 1350 cm^{-1}, and 2D band at ~2690 cm^{-1} correspond to 1) in-plane vibrational mode involving sp^2 hybridized carbons (G band), 2) disordered mode induced sp^3-bonded carbons from edges of graphene (D band), 3) the amount of graphitic layers (2D band) [56]. Therefore, graphite which has just low D/G ratio indicates just small amounts of defects in graphite flakes as well as a high degree of sp^2 bond crystallinity. But significant amounts of graphitic layers and sp^2 bonds are destroyed during the oxidation processes. This destruction results in relatively high D/G ratio in GO samples. The ratio of D/G again decreases with the reduction process of GOs by recovering graphitic structures.

While the 2D band does not represent defects in the graphene structure, both band position and band shape are affected by the number of graphene layers in the structure. Heavily oxidized graphene also makes the 2D band low and be indistinguishable. The broad and low intensity of the 2D band of PEDOT:PSS/GO(05) implies that the amount of potassium permanganate was not enough to oxidize and to exfoliate the graphite sufficiently. Furthermore, indistinguishable 2D peaks of PEDOT:PSS/GO(15) and PEDOT:PSS/GO(25) are originated from the excessive oxidation of graphitic structures. From the Raman spectra of rGO, it is observed that recovering sp^2 carbons makes the 2D peaks relatively sharp and distinguishable.

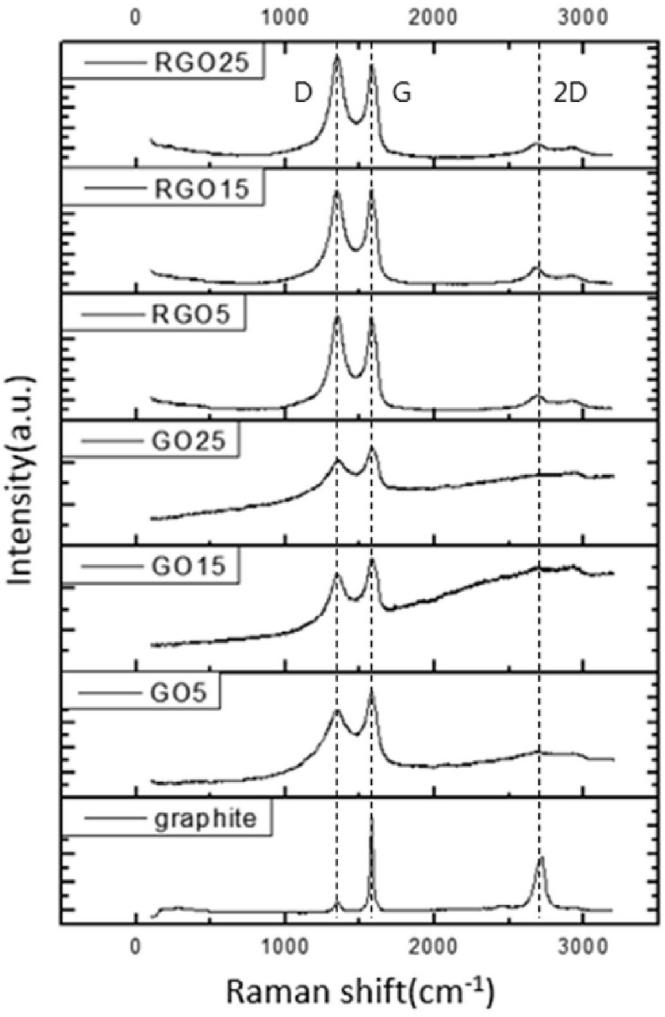

Fig. 2. Raman spectra of graphite, GOs, and rGOs.

3.2. Electrochemical deposition of PEDOT composites

PEDOT:PSS, PEDOT:PSS/GO and PEDOT:PSS/rGO composite films were successfully deposited on the gold micro-electrodes (7.85×10^{-3} mm^2) by a chronopotentiometry method (5 μA, 3 min). During the PEDOT deposition, the surface of electrodes was covered with dark colored composites (Fig. 1(c)) and the voltages

Table 1
Primer design for target gene sequence.

Target gene	Forward primer	Reverse primer
rGAP-43	AAG CTG AGG AGG AGA AAG AA	GCA TGT TCT TGG TCA GCC
rSynapsin-1	CCA ATC ATA AAG AGA TGC TC	CAA TAT CCT GGA AGT CAT GT
rBeta actin	CCG TGA AAA GAT GAC CCA GA	GTC TCC GGA GTC CAT CAC AA

was gradually increased from 1.8 V to 2.0 V. (SFig. 1) Even if the PEDOT composites have lowered the electrochemical impedance of the Au electrode, its electrical resistivity in dry state could be a little higher measured than the Au itself. The morphology of the coated PEDOT composites was compared by SEM images (Fig. 3). While PEDOT:PSS showed typical polymeric smooth surfaces at the submicron scale, the GO and rGO composites clearly showed microscale particulates or sheets by the degree of oxidation and exfoliation of GOs. We also have performed the EDS analysis of PEDOT:PSS/graphene composites. While there are some significant variations in oxygen contents, it is quite complex to draw a systematic conclusion because oxygen contents are complex functions of 1) ratio between PEDOT:PSS and GOs/rGOs, 2) redox degrees of GOs, and 3) residual water in porous structures. One note is that some degree of decrement in oxygen contents is clearly shown by changing from GOs to rGOs. The detailed analysis data were presented in the Supplementary Information as in Fig. S2.

3.3. Electrochemical performances of PEDOT:PSS/GO composites

EIS, CV, BPSs and durability tests were performed to evaluate the electrochemical performances of the PEDOT:PSS/GO composites for the neural electrode. The EIS results show that PEDOT coating reduces the impedances of the electrodes from the bare gold in wide frequency ranges, particularly from 4000–1 Hz(Fig. 4). Given that the neural action potential has around 0.1–1 kHz, the impedance at 1 kHz should be a key parameter for estimating the performances of neural recording sensitivity as well as occurring potentials for neural stimulation. The impedances at 1 kHz of all the PEDOT composites was reduced more than 27% compared to the bare gold electrode. Note that the improvements in impedances of PEDOT:PSS come from the nano-porous structures to increase the active surface area to transfer charges from electrons to ions. However, the further impedance reduction by filling GO/rGO is because of improved electrical charge conduction through rather bulky porous structures of PEDOT:PSS/GO and PEDOT:PSS/rGO composites. Other variables affecting impedances come from the degrees of oxidation and exfoliation whose electrical contributions are exerting conversely. While more oxidization might result in higher exfoliation of graphite, a higher degree of exfoliation improves the effectiveness of dispersing conductive GOs/rGOs in the composites so that electrical properties of GO composites improve with a high degree of exfoliation of graphite. Thus, the impedance varied by the degree of oxidation as well as redox states of GOs together. Overall, the impedance of the PEDOT:PSS/rGO(15) was the lowest among all the composites.

For comparing the PEDOT:PSS/rGO composites, however, another complexity, the degree of recovered conjugated carbons, also involves in affecting the impedances. The high degree of oxidation sacrifices electrical properties of graphene when it is reduced. Because electrical conduction on a graphitic layer is primarily dependent on the crystallinity of sp^2 conjugated carbon. Obviously, in the Raman analysis, GO(25) has a higher degree of oxidation than GO(15) by comparing D bands. While the impedance of PEDOT:PSS/rGO(15) decreased to $0.59 \pm 0.27\,\Omega\,cm^2$ dramatically from PEDOT:PSS/GO(15) which has $1.24 \pm 0.35\,\Omega\,cm^2$, the impedance of PEDOT:PSS/rGO(25) was similar to PEDOT:PSS/GO(25) which are $1.01 \pm 0.25\,\Omega\,cm^2$ and $1.00 \pm 0.30\,\Omega\,cm^2$ respectively. Probably, GO(25) became too much oxidized for conductive carbon structures to be recovered effectively again. For GO(05), since the exfoliation by oxidation did not occur sufficiently, the effect of reduction was not remarkable. That is why the impedances of PEDOT:PSS/GO(05) and PEDOT:PSS/rGO(05) were similar to be $1.29 \pm 0.27\,\Omega\,cm^2$ and $1.28 \pm 0.32\,\Omega\,cm^2$ at 1 kHz, respectively.

The impedance spectra can be fitted to an equivalent circuit model to interpret their electrochemical charge transport phenomena further [72]. One suggested circuit model for conducting polymer coating is comprised of the Solution resistance ($\mathbf{R}_s$), substrate resistance ($\mathbf{R}_{sub}$), substrate capacitance ($\mathbf{C}_{sub}$), coating resistance ($\mathbf{R}_{coa}$), coating capacitance ($\mathbf{C}_{coa}$), the semi-infinite Warburg diffusion impedance ($\mathbf{Z}_D$) and constant phase element (CPE) ($\mathbf{Z}_Q$) as shown in Fig. 5. The EIS parameters were calculated by the fitting of impedance spectra to the equivalent circuit model in Table 2. The semi-infinite Warburg diffusion impedance ($\mathbf{Z}_D$) and constant phase element ($\mathbf{Z}_Q$) are calculated by the following formula, respectively.

$$\boldsymbol{Z}_D = \frac{1}{Y_0\sqrt{(j\omega)}}$$

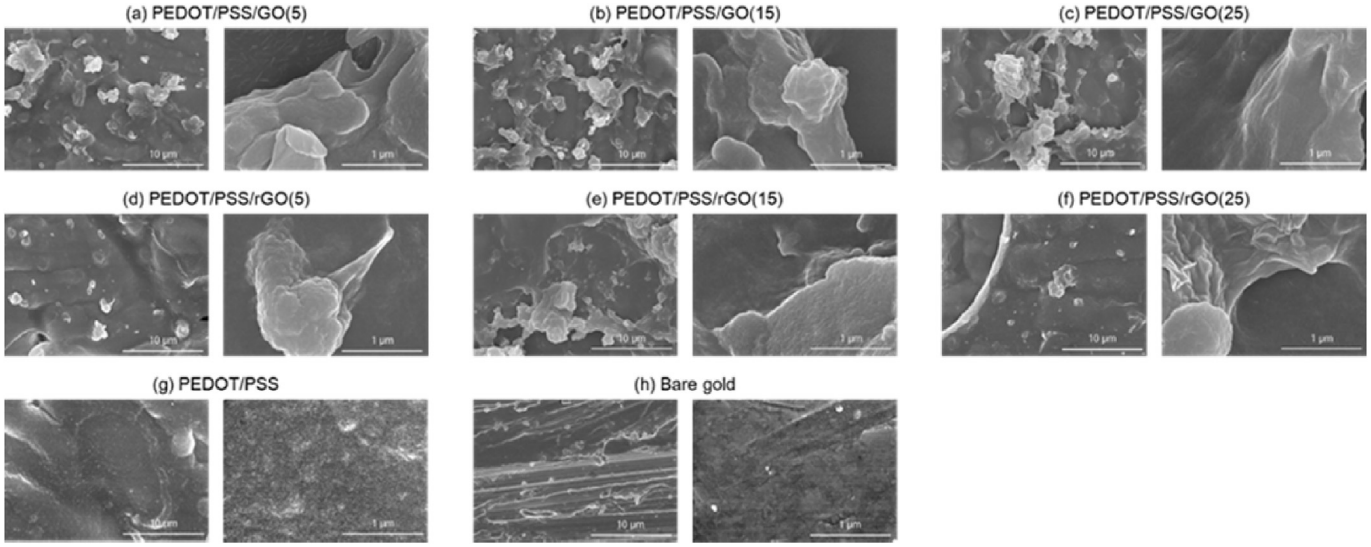

Fig. 3. SEM images of (a) PEDOT/PSS/GO(05), (b) PEDOT/PSS/GO(15), (c) PEDOT/PSS/GO(25), (d) PEDOT/PSS/rGO(05), (e) PEDOT/PSS/rGO(15), (f) PEDOT/PSS/rGO(25), (g) PEDOT/PSS and (h) Bare gold.

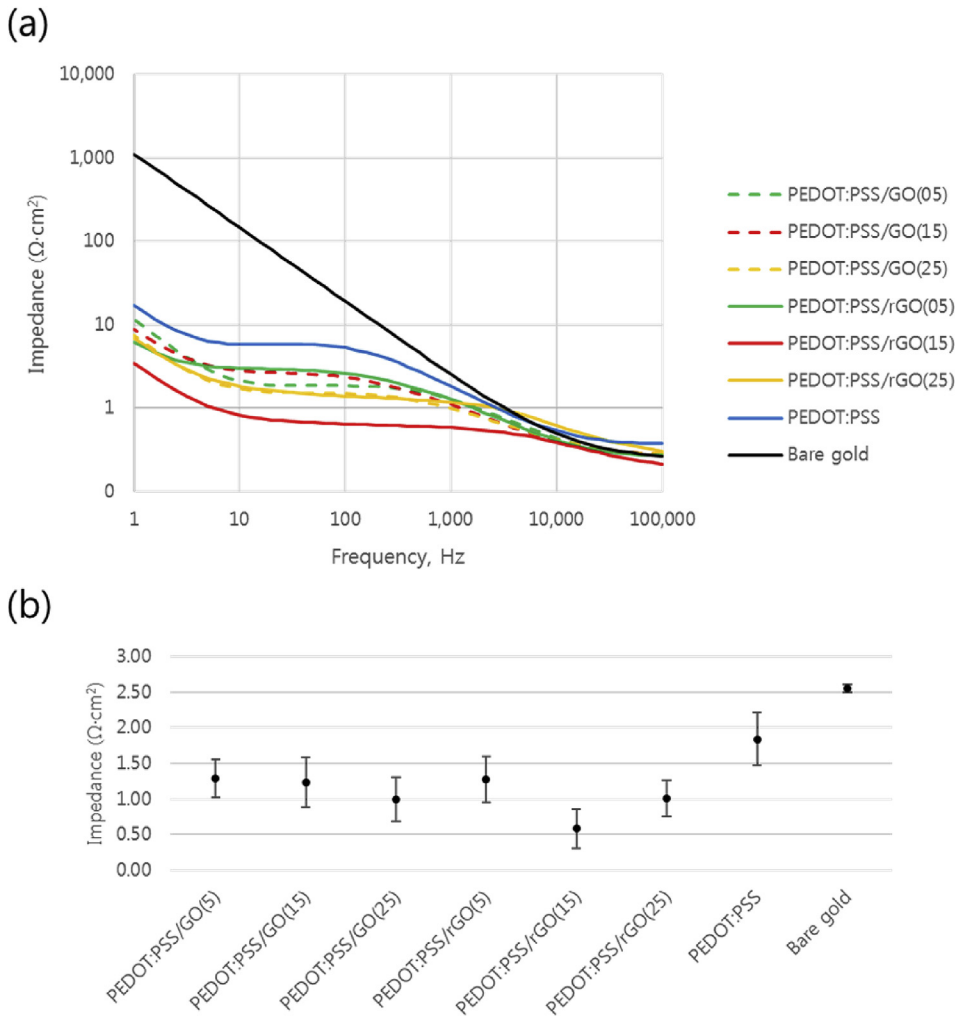

Fig. 4. Electrochemical impedance spectroscopy of PEDOT composites. (a) Bode plot and (b) impedance at 1 kHz. Each data point represents the average of five electrodes with standard deviation. (n = 5).

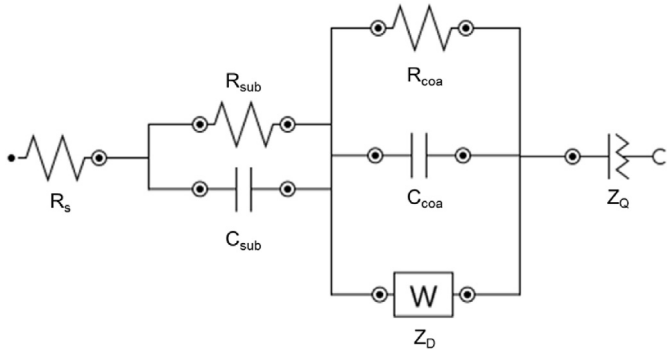

Fig. 5. Equivalent circuit model for PEDOT:PSS/graphene composites. Solution resistance ($\mathbf{R}_s$), substrate resistance ($\mathbf{R}_{sub}$), substrate capacitance ($\mathbf{C}_{sub}$), coating resistance ($\mathbf{R}_{coa}$), coating capacitance ($\mathbf{C}_{coa}$), semi-infinite Warburg diffusion impedance (Z_D) and constant phase element ($\mathbf{Z}_Q$).

$$\boldsymbol{Z}_Q = \frac{1}{Y_0(j\omega)^n}$$

$\mathbf{Y}_0$ is the admittance of an ideal capacitance. And n is an empirical constant ranging from 0 to 1. When n = 1, the $\mathbf{Z}_Q$ behaves as a pure capacitor, while when n = 0, the $\mathbf{Z}_Q$ behaves a pure resistor. Further, when n = 0.5, the $\mathbf{Z}_Q$ is the equivalent of the Warburg element. For all the GO and rGO composites, the n was approaching to 1. While deciphering the circuit model to the actual physical phenomena seems to be extremely difficult because of the limitation of our understanding of the system, only a few things can be highlighted. The solution resistances, which might depend on the distance among the working, the counter, and the reference electrodes as well as the dissolved ionic concentrations, are well confined in the ranges of 2.60–3.62 kΩ. This consistency confirms that our experimental set-up was well constructed to test the performances of the composites. The other noticeable fact is that the constant phase element (CPE) admittance, $\mathbf{Y}_{0dl}$ related to the behavior of double layer increased by reduction of GOs through the hydrodynamically resistive porous structures of PEDOT composites ($\mathbf{R}_{coa}$). This improved $\mathbf{Y}_{0dl}$ allows to increase CSC as well as to reduce faradaic side reactions. While the desired neural interfaces require to transfer electrical charges solely by physical mechanisms, pseudocapacitive transports, at the surface of PEDOT:PSS/GO or rGO composites, evidently there should exist substantial degrees of chemical redox reactions ($\mathbf{C}_{coa}$) which cause faradaic charge injections along with the interfaces without diffusion. This combination of physical and chemical mechanisms makes the composite system too complex to analyze in a single model. Thus, the physical

Table 2
EIS parameters obtained by fitting of impedance spectra to the equivalent circuit model.

Element	Parameter	PEDOT:PSS/GO(05)	PEDOT:PSS/GO(15)	PEDOT:PSS/GO(25)	PEDOT:PSS/rGO(05)	PEDOT:PSS/rGO(15)	PEDOT:PSS/rGO(25)
		Value	Value	Value	Value	Value	Value
R_s	R_s(kΩ)	2.78 ± 0.04	2.60 ± 0.10	3.62 ± 0.14	3.15 ± 0.06	3.62 ± 0.09	3.54 ± 0.07
R_{sub}	R_{sub}(kΩ)	1.32 ± 0.13	1.82 ± 0.37	1.77 ± 0.34	1.40 ± 0.23	1.85 ± 0.09	1.44 ± 0.09
C_{sub}	C_{sub}(nF)	9.92 ± 0.85	4.84 ± 0.77	4.29 ± 0.88	7.44 ± 0.94	1.31 ± 0.14	2.24 ± 0.24
R_{coa}	R_{coa}(kΩ)	32.74 ± 0.70	10.89 ± 0.70	16.31 ± 0.80	37.50 ± 0.81	53.98 ± 0.40	41.27 ± 0.35
C_{coa}	C_{coa}(nF)	11.01 ± 0.52	9.75 ± 1.72	7.76 ± 1.06	5.68 ± 0.34	1.57 ± 0.03	2.19 ± 0.05
Z_D	Y_{0coa}(μS·$s^{1/2}$)	0.36 ± 0.03	0.15 ± 0.11	0.18 ± 0.07	0.22 ± 0.02	0.10 ± 0.00	0.10 ± 0.00
Z_Q	Y_{0dl}(μS·s^n)	1.17 ± 0.03	1.27 ± 0.06	1.16 ± 0.06	1.96 ± 0.09	3.18 ± 0.08	1.71 ± 0.03
	n	1.01 ± 0.01	1.02 ± 0.02	1.03 ± 0.02	1.03 ± 0.02	0.88 ± 0.01	0.93 ± 0.01
	χ^2	0.0415	0.2121	0.1852	0.0632	0.0108	0.0133

R_s: solution resistance.
R_{sub}: substrate resistance.
C_{sub}: substrate capacitance.
R_{coa}: coating resistance.
C_{coa}: coating capacitance.
Y_{0coa}: admittance of Warburg element.
Y_{0dl}: admittance of double layer capacitor.
Z_Q: constant phase element.
χ^2: Chi-Squared goodness of fit.

interpretation of the equivalent circuit model becomes fuzzy now. This elemental study should be further performed by isolating the parameters involved.

To evaluate the CSC of the composites, CV analysis has been performed in the range of applied potential from −0.6 V to 0.8 V (Fig. 6). PEDOT:PSS has been known to increase CSC from the bare gold electrode by forming porous ionic storage channels along with the molecular structures of PEDOT. We obtained the CSC of

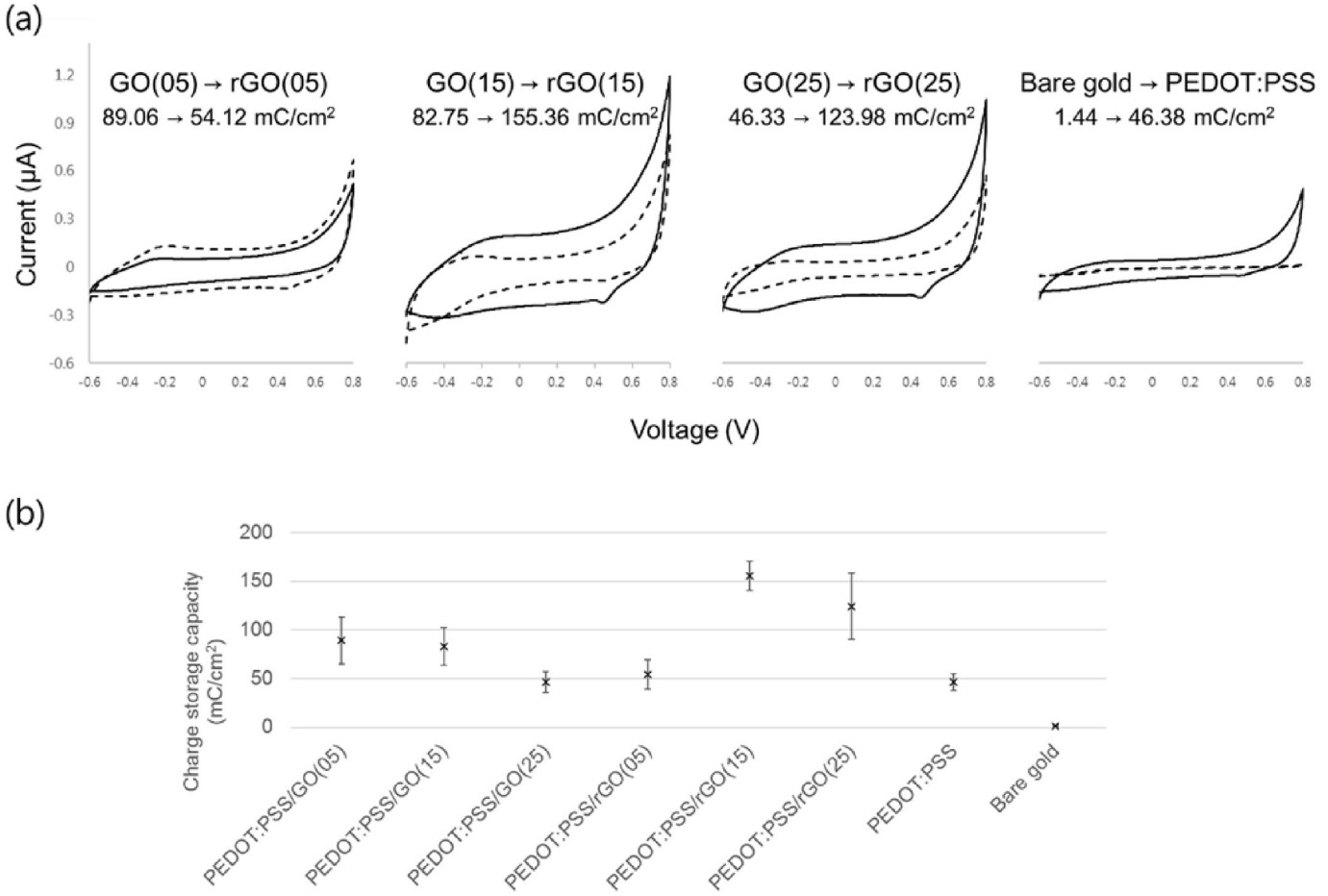

Fig. 6. (a) Cyclic voltammogram of bare gold, PEDOT:PSS, GO and rGO composites. The GOs and bare gold are expressed as the dashed line, and the rGOs and PEDOT:PSS are expressed as the solid line. The charge storage capacity is displayed on each graph. (b) Calculated charge storage capacity from cyclic voltammogram. Each data point represents the average of five electrodes with standard deviation. (n = 5).

$46.38 \pm 8.82\ mC/cm^2$ for PEDOT which is well matched to the typical level of CSC for PEDOT coated microelectrode. (38–78 mC/cm^2) [52,57,58] Evidently, CSCs have increased by adding GOs in the composites. Moreover, their CSCs have further improved by rGOs. While the maximum CSC, $155.36 \pm 14.83\ mC/cm^2$, has been obtained with PEDOT:PSS/rGO(15), the PEDOT:PSS/rGO(15), and rGO(25) have improved 187.74% and 267.58% from its corresponding PEDOT:PSS/GO composite, respectively. Because the conductivities of rGOs are higher than those of GOs, the PEDOT:PSS/rGO composites have fully active charge transfer sites along with the porous and bulky composite structures and thus, higher CSCs are obtained. Note that rGO(25) has resulted in relatively low CSC value than rGO(15) because of too much destruction of conduction paths by overoxidation. These high CSCs on the electrodes are important parameters for neural interfaces. The higher CSCs can be interpreted as one of the indications of ability to protect both biotic and abiotic system by reducing chances of faradaic charge injection which inevitably involves electrochemical reactions. Thus, PEDOT:PSS/rGO composites show partly favorable electrochemical performances as neural interfaces.

To understand the electrochemical meaning of CSCs in detail, we have compared the calculated parameters from the equivalent circuit model in Fig. 5 and the CSC values in Fig. 6. Voluminous PEDOT:PSS/GO provides rather fuzzy ionic charge transfer and charge diffusion phenomena on the electrode, which can be difficult to be interpreted solely by perfect capacitance units. We found out that CPE (Z_Q) and the coating resistance (R_{coa}) show the trends well matched to the CSCs. Because CPE represents imperfect capacitance unit, the well-matched trends explain that the CSCs involve the behaviors of a double layer in the hydrodynamically resistive microstructures.

Electrochemical symmetric BPS responses of the PEDOT:PSS/GO or rGO composites, PEDOT:PSS, and Au electrodes were evaluated by measuring the invoked potential for 500 μs at each phase and 200 μs between phase. Because higher invoked potential may cause unwanted reactions on either solutions and biotic materials systems, particularly neural tissues, BPS performances can be a direct indication for evaluating the safety of stimulating electrodes as neural interfaces. Furthermore, the rapid recovery from the voltage spike at interval allows higher frequency stimulation [59]. From the BPS, the charge injection limits (CIL) were calculated (Fig. 7). When the maximum cathodal excursion potential is reached to −0.6 V which is potential window safely used in neural stimulation, the delivered charges can be calculated from the applied current. As expected, the PEDOT:PSS/rGO(15) showed the highest CIL. It also has lower impedances at around 100–1000 Hz as well as higher CSC. However, CIL trends of whole samples were not exactly matched to the order of the performances of CSCs and EISs. While all the PEDOT and PEDOT composite coated electrodes showed much safe voltage invoking performances compared to the bare gold electrode, particularly PEDOT:PSS/rGO(15) and PEDOT:PSS/rGO(25) showed much higher CIL due to increased amounts of charge carriers [58]. Furthermore, these samples showed pretty constant areas of the applied voltage measured relative to the open circuit voltage.

When the charges are injected from the neural electrodes with low CIL, the unrecovered voltage in the interphase gap can be accumulated by repeating cycles. It triggers continuous voltage drifts in the following cycles, and thus this accumulation could be harmful to the neural tissue if the total voltage drift reaches to a certain level. If the area changes, then we can assume that there exist some unwanted side reactions which might be fairly irreversible during neural stimulation [60].

The electrochemical durability tests were performed in a phosphate buffer solution with the harsh voltage range, ±1 V for 500 cycles (Fig. 8 and Table 3). Because conducting polymers are swelling and contracting by repeating cyclic voltammetry, their electrochemical performances can degrade gradually, particularly in a high potential range. We have chosen ±1 V for testing durability against corrosion because this invoked potential range can be a harsh limit at the surface of electrodes for neural stimulation. The 1st cycle of our samples shows higher CSC value than both 100^{th} and 500^{th} cycles except the bare gold electrode. After 500^{th} cycles, the diameter of the bare gold electrode increased from 100 μm to 120–130 μm, which implies dissolution and complex deposition of gold. By repeating CV for 500 times, the CSC of PEDOT:PSS has changed from $33.55 \pm 2.06\ mC/cm^2$ to $9.77 \pm 2.13\ mC/cm^2$ while all the PEDOT:PSS/GO or rGO composites also have experienced the similar severe drops in CSCs. In this condition, the working electrode system seems to have some side reaction such as

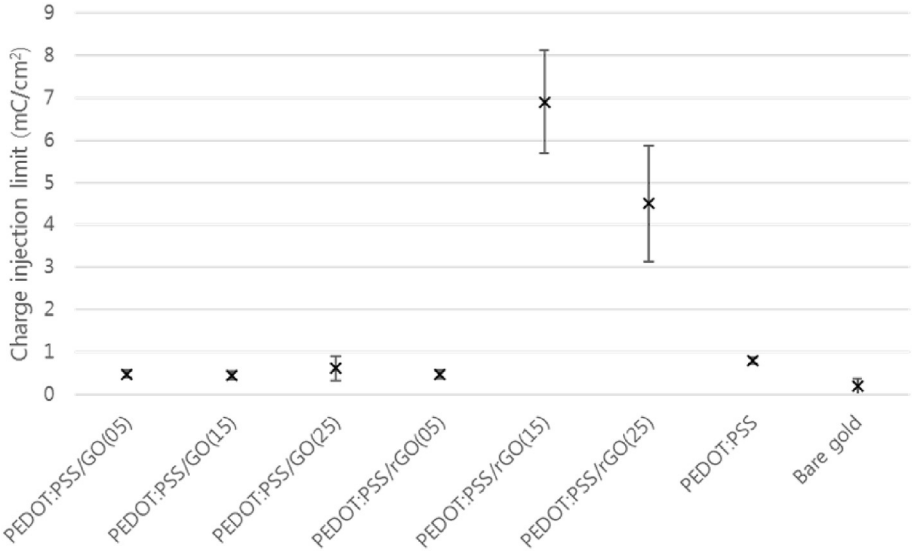

Fig. 7. Charge injection limit for PEDOT:PSS, bare gold and GO and rGO composites. Pulse and phase widths were 500 μs and 200 μs respectively. Each data point represents the average of five electrodes with standard deviation. (n = 5).

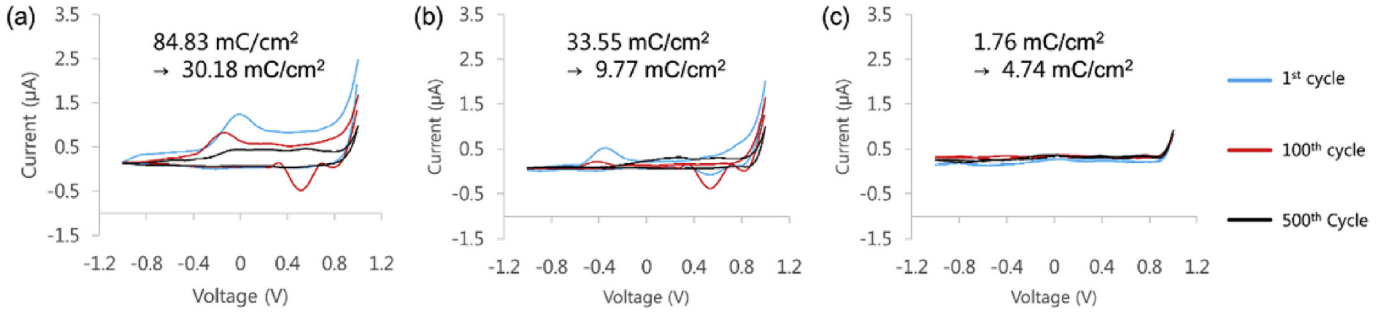

Fig. 8. Electrochemical durability test results of (a) PEDOT:PSS/rGO(15), (b) PEDOT:PSS, (c) Bare gold with sweep range of −1.0–1.0 V. Each inset text indicates CSC values before and after 500 cycles. (For interpretation of the references to color in this figure legend, the reader is referred to the Web version of this article.)

Table 3
Charge storage capacity measured at 1st, 100th and 500th cycle.

Sample name	CSC as-prepared (mC/cm^2)	Relative value to as-prepared (%)	CSC after 100 cycles (mC/cm^2)	Relative value to as-prepared (%)	CSC after 500 cycles (mC/cm^2)	Relative value to as-prepared (%)
1. PEDOT:PSS/GO(05)	33.11 ± 1.67	100	20.94 ± 3.13	63.3	18.21 ± 1.79	54.9
2. PEDOT:PSS/GO(15)	47.63 ± 3.11	100	42.60 ± 3.62	89.5	21.51 ± 0.62	45.2
3. PEDOT:PSS/GO(25)	41.80 ± 2.64	100	40.31 ± 0.93	96.5	28.08 ± 7.23	67.2
4. PEDOT:PSS/rGO(05)	94.83 ± 3.80	100	42.32 ± 2.45	44.6	32.90 ± 1.95	34.7
5. PEDOT:PSS/rGO(15)	84.83 ± 2.25	100	60.63 ± 1.71	71.5	30.18 ± 3.57	35.6
6. PEDOT:PSS/rGO(25)	56.23 ± 5.13	100	22.16 ± 2.97	39.4	26.10 ± 4.54	46.4
7. PEDOT:PSS	33.55 ± 2.06	100	18.54 ± 2.22	55.3	9.77 ± 2.13	29.1
8. Bare gold	1.76 ± 0.72	100	3.98 ± 1.55	226.1	4.74 ± 0.89	269.1

overoxidation. However, note that the residual CSCs after 500 cycles of PEDOT:PSS/GO or rGO composites were higher (34.70–67.19%) than that of PEDOT:PSS (29.12%). In particular, the PEDOT:PSS/GO composites showed slower CSC decrement than rGO composites. It means that the adhesion of GOs to the PEDOT:PSS are better than rGOs. Nevertheless, since the initial CSCs of rGO composites were far higher than that of GO composites, the CSCs after 500 cycles were maintained high. This result confirms that both the adhesion of GO and rGO composites to the gold surface and the electrochemical durability of those against corrosion were significantly improved from the PEDOT:PSS.

3.4. Mechanical analysis

The nanoindentation measurement was used to analyze the mechanical softness of PEDOT:PSS/GO or rGO composites (Fig. 9). The samples for analysis were synthesized on the ITO coated glass to be made with a large area. The indentation was operated with a depth of 0–40–100 nm, and the average moduli were calculated over a range of 20–30 nm depth to obtain reliable data. The average modulus of PEDOT:PSS was measured at 7.30 ± 0.50 GPa. However, while the PEDOT:PSS/GO or rGO composites include extremely rigid nanofillers whose modulus are in the range of hundreds to thousand GPa, it was surprisingly measured to be in the range of 2–5 GPa which is much lower than that of PEDOT:PSS itself. Briefly, more GO content and higher reduced states caused softer modulus properties. This inclination of the composites is extremely unusual if our composite is homogeneous mixtures of PEDOT and GO. However, as stiff nano carbons are included more in the composites, it appears that the PEDOT forms far more irregular nanostructures with pores which might cause desirable ion flowing

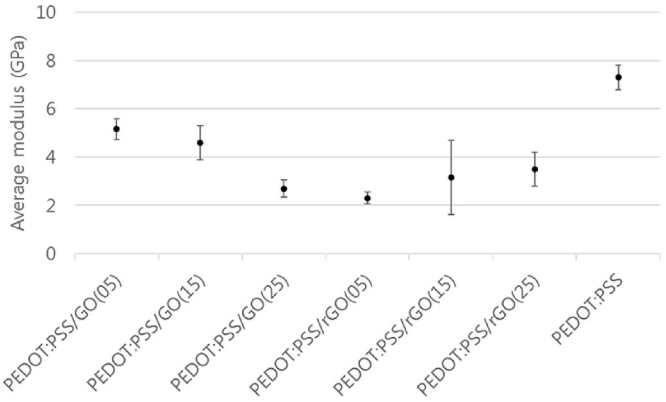

Fig. 9. Average modulus of PEDOT:PSS, PEODT:PSS/GO and rGO composites measured by nanoindentation. The modulus was collected in 20–30 nm depth region.

highways as well as mechanical softness. Thus, the PEDOT:PSS/rGO(15) composite showed the concurrent desirable behaviors in both electrochemical and mechanical performances as soft implantable electrodes.

3.5. PC12 neural cell tests

To analyze cytocompatibility of PEDOT composites, cell viability, growth of neurite, the gene expressions of PC12 neural cell lines have been tested by comparing PEDOT:PSS, PEDOT:PSS/GO and rGO composites, and ITO glass. Firstly, the cell viability of PC12 cells on the surface of PEDOT composites was tested (Fig. 10). There was not much noticeable difference in PC12 cell viabilities among the

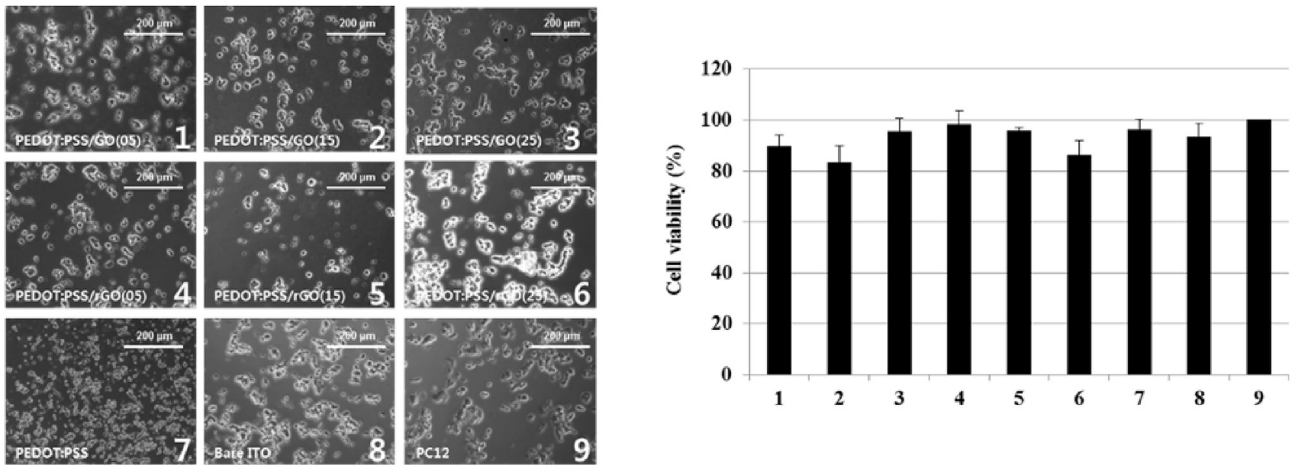

Fig. 10. Cell viability on the surface of PEDOT:PSS/GO composites. (a) Living PC12 cell images were shown by 20× magnification. (b) Cell viability of PC12 cells were measured by the CCK-8 assay.

PEDOT composites, PEDOT:PSS, and ITO glass at around 85–95%. This indicates that GO or rGO composites of PEDOT play insignificant effects on the performance of holding PC12 cells on their surfaces while PEDOT:PSS itself is a little poorer than the non-conductive polystyrene (PS) surface of the cell culture flask.

In Fig. 11 (a) and (b), neurite growth results of the PC12 cells were compared. After treating with collagen and nerve growth factor (NGF) for 7 days, the neurite lengths were directly observed by optical microscope and directly measured. The neurites on the conductive surfaces were clearly longer than those on the non-conductive PS well plate. The longest neurite formation among the tested was 98.7 μm on the PEDOT:PSS/rGO(15) and 85.3 μm on the PEDOT:PSS/GO(05) was the second longest, which at least excels PEDOT:PSS and even ITO conductive surface.

The relative gene expression of GAP-43 and synapsin on the surface of PEDOT composites were also compared in Fig. 8(c) and (d). The GAP-43 is a neural specific cytoplasmic protein which is related to axonal membrane regeneration. This protein plays a key role in neurite outgrowth, regeneration, and plasticity [61,62]. Furthermore, the expression of phosphoprotein GAP-43 which is an endogenous substrate for protein kinase C is stimulated by NGF, and the up-regulation of GAP-43 mRNA and protein increases during the differentiation of PC12 cells into the neuronal phenotype [63,64]. The expression of GAP-43 in PC12 cells is promoted on a

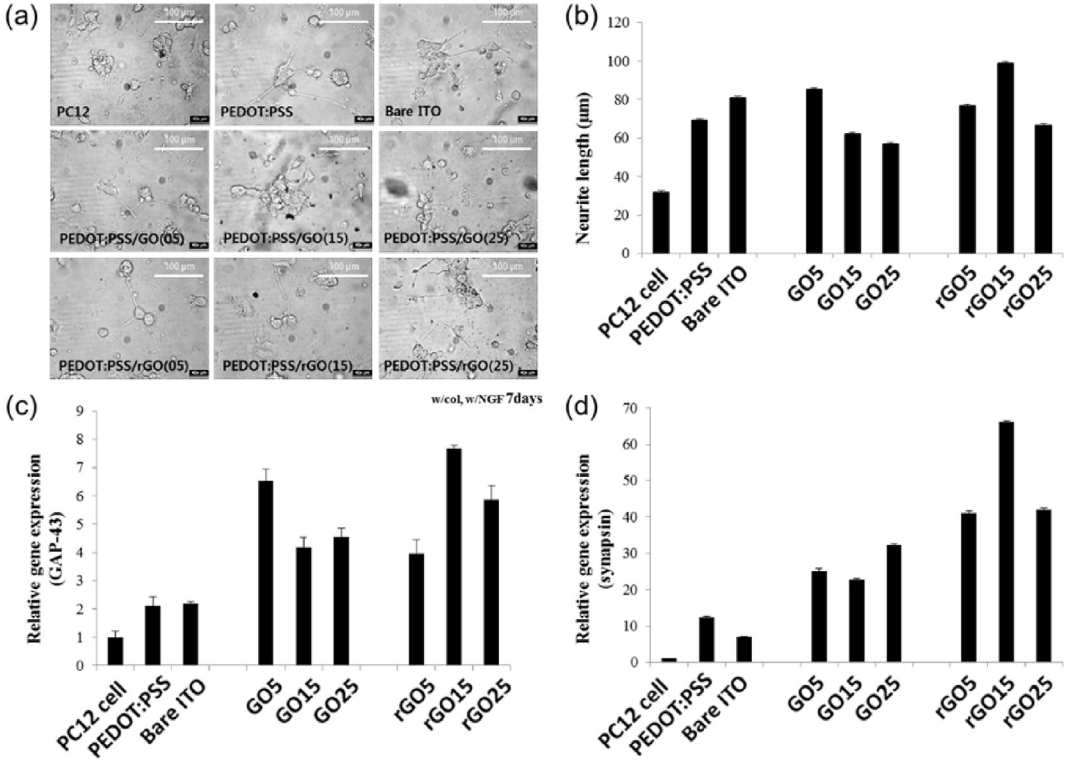

Fig. 11. (a) Microscopic images of the PC12 cells on the surface of PEDOT composites after treated with collagen and neurite growth factor for 7 days. The images were magnified by 40×. (b) Measured neurite length and relative gene expression of (c) GAP-43 and (d) synapsin of PC12 cells were compared on the prepared PEDOT:PSS/GO composites.

conductive surface such as graphene [65] and promoted further by electric field application even on a non-conductive surface [66]. The surface modification of graphene oxide with the acetylcholine-like unit could promote GAP-43 expression effectively [67]. In this study, the relative gene expression of GAP-43 of PC12 on the surfaces of the PEDOT:PSS/GO and rGO composites were significantly higher than the well plate, ITO coated glass, and PEDOT:PSS. While the PEDOT:PSS and ITO showed more than two times of the GAP-43 expression compared to the well plate, the PEDOT:PSS/GO and rGO composites showed much improved GAP-43 expression compared to the ITO and PEDOT:PSS. Particularly PEDOT:PSS/rGO(15) showed the highest GAP-43 expression, which is 7.7 times higher than that of the well plate. These result is significantly higher value than the graphene-only substrates [65,67]. The high GAP-43 expression implies that the PEDOT:PSS/GO or rGO composites hold beneficial potentials, for examples, 1) to induce static neural regeneration, 2) to shorten the distance between the neural electrode and neurons by inducing axonal membrane regeneration of neural cells when applied *in vivo*, 3) to overcome synkinesis.

Synapsin is abundant pre-synaptic phosphoprotein associated with the cytoplasmic side of synaptic vesicles which have the capacity to promote actin polymerization and to stimulate cell differentiation [68–71]. These synapsin expressions among PEDOT composites were much more dramatic than those of GAP-43. While the synapsin expressions on all the conductive surfaces were at least 7 times higher than that of the well plate, PEDOT:PSS and PEDOT:PSS/GO composites were about 1.7 times and 3.2–4.6 times higher than that of the ITO coated glass, respectively. Furthermore, the PEDOT:PSS/rGO composites showed better synapsin expression than any of the PEDOT:PSS/GO composites. Among them, PEDOT:PSS/rGO(15) has shown the highest synapsin expression which is at least 2.1 times higher than any of the PEDOT:PSS/GO composites, ~9.4 times and ~66 times higher than ITO and the well plate, respectively. Though PEDOT or graphene-related materials on promoting synapsin expression have not been found in any previously reported paper, there is a report showing that polypyrrole(PPy)-coated poly (L-lactic acid-co-caprolactone)/silk fibroin could do [66]. Moreover, our PEDOT composites showed a slightly higher value than the PPy composites. Because higher synapsin expression could provide more potential to induce dynamic intercellular communication, our PEDOT:PSS/GO or rGO composites will have a unique impact on solving synkinesis, long-distance cut, and chronic cut issues in regenerating neural tissues. Furthermore, these favorable gene expressions in regenerating neural tissues as well as axonal neurite have beneficial contribution to developing intelligent neural interfaces.

4. Conclusion

In this research, the soft PEDOT:PSS/GO and PEDOT:PSS/rGO composites were electrochemically deposited on the Au microelectrodes. The electrochemical performances of PEDOT:PSS/rGO composites were much higher than PEDOT:PSS and the bare gold micro-electrode in terms of impedance, CSC, CIL, and durability while showing softer modulus. From *in vitro* PC12 neural cell tests, the PEDOT:PSS/GO or rGO composites was proven to be not only cytocompatible by the cell viability evaluation, but also able to modulate important gene expressions of specific proteins such as GAP-43, regulating axonal regeneration, and synapsin, enhancing intercellular communications. This gene expression implies that the PEDOT:PSS/GO or rGO composites can play unique roles to overcome long-lasting challenges in regenerating neural tissues, such as synkinesis, long-distance cut, and long-term cut. Thus, our PEDOT:PSS/GO or rGO composites will make them strong candidates among conductive biomaterials for the applications of an implantable electrode, biosensors, bio-actuators, drug delivery carriers, and neural interfaces.

Acknowledgments

This work was funded by Nation Research Foundation of Korea (Basic Research Program: NRF-2017R1A2B4012736, 2018R1A6A1A03025523, 2017R1A2A2A07001272, Korea NRF-US AFRL AFOSR Joint Program: NRF-2018K1A3A1A32055149).

Appendix A. Supplementary data

Supplementary data to this article can be found online at https://doi.org/10.1016/j.electacta.2019.04.099.

References

[1] L.R. Hochberg, D. Bacher, B. Jarosiewicz, N.Y. Masse, J.D. Simeral, J. Vogel, S. Haddadin, J. Liu, S.S. Cash, P. van der Smagt, J.P. Donoghue, Reach and grasp by people with tetraplegia using a neurally controlled robotic arm, Nature 485 (7398) (2012). 372-U121.
[2] L.R. Hochberg, M.D. Serruya, G.M. Friehs, J.A. Mukand, M. Saleh, A.H. Caplan, A. Branner, D. Chen, R.D. Penn, J.P. Donoghue, Neuronal ensemble control of prosthetic devices by a human with tetraplegia, Nature 442 (7099) (2006) 164–171.
[3] G.G. Wallace, S.E. Moulton, G.M. Clark, Electrode-cellular interface, Science 324 (5924) (2009) 185–186.
[4] P. Krack, A. Batir, N. Van Blercom, S. Chabardes, V. Fraix, C. Ardouin, A. Koudsie, P.D. Limousin, A. Benazzouz, J.F. LeBas, A.L. Benabid, P. Pollak, Five-year follow-up of bilateral stimulation of the subthalamic nucleus in advanced Parkinson's disease, N. Engl. J. Med. 349 (20) (2003) 1925–1934.
[5] W.H.a.F. Theodore, R.S, Brain stimulation for epilepsy, Lancet Neurol. 3 (2004) 111–118.
[6] S.M. Klein, M.S. Melton, W.M. Grill, K.C. Nielsen, Peripheral nerve stimulation in regional anesthesia, Reg. Anesth. Pain Med. 37 (4) (2012) 383–392.
[7] J. Schoenen, L. Di Clemente, M. Vandenheede, A. Fumal, V. De Pasqua, M. Mouchamps, J.M. Remacle, A.M. de Noordhout, Hypothalamic stimulation in chronic cluster headache: a pilot study of efficacy and mode of action, Brain 128 (2005) 940–947.
[8] H.S. Mayberg, A.M. Lozano, V. Voon, H.E. McNeely, D. Seminowicz, C. Hamani, J.M. Schwalb, S.H. Kennedy, Deep brain stimulation for treatment-resistant depression, Neuron 45 (5) (2005) 651–660.
[9] K. Famm, B. Litt, K.J. Tracey, E.S. Boyden, M. Slaoui, A jump-start for electroceuticals, Nature 496 (7444) (2013) 159–161.
[10] S.F. Cogan, Neural stimulation and recording electrodes, Annu. Rev. Biomed. Eng. 10 (2008) 275–309.
[11] S. Budday, R. Nay, R. de Rooij, P. Steinmann, T. Wyrobek, T.C. Ovaert, E. Kuhl, Mechanical properties of gray and white matter brain tissue by indentation, J. Mech. Behav. Biomed. Mater. 46 (2015) 318–330.
[12] E. Patrick, M.E. Orazem, J.C. Sanchez, T. Nishida, Corrosion of tungsten microelectrodes used in neural recording applications, J. Neurosci. Methods 198 (2) (2011) 158–171.
[13] S.K. Lee, H. Kim, B.S. Shim, Graphene: an emerging material for biological tissue engineering, Carbon letters 14 (2) (2013) 63–75.
[14] S. Baek, R.A. Green, L.A. Poole-Warren, Effects of dopants on the biomechanical properties of conducting polymer films on platinum electrodes, J. Biomed. Mater. Res. A 102 (8) (2014) 2743–2754.
[15] U. Lang, J. Dual, Mechanical Properties of the Intrinsically Conductive Polymer Poly (3, 4-ethylenedioxythiophene) Poly (styrenesulfonate)(PEDOT/PSS). Key Engineering Materials, vol. 345, Trans Tech Publications, 2007, pp. 1189–1192.
[16] J. Qu, L. Ouyang, C.-c. Kuo, D.C. Martin, Stiffness, strength and adhesion characterization of electrochemically deposited conjugated polymer films, Acta Biomater. 31 (2016) 114–121.
[17] X.Y. Cui, D.C. Martin, Electrochemical deposition and characterization of poly(3,4-ethylenedioxythiophene) on neural microelectrode arrays, Sensor. Actuator. B Chem. 89 (1–2) (2003) 92–102.
[18] S.M. Richardson-Burns, J.L. Hendricks, B. Foster, L.K. Povlich, D.H. Kim, D.C. Martin, Polymerization of the conducting polymer poly(3,4-ethylenedioxythiophene) (PEDOT) around living neural cells, Biomaterials 28 (8) (2007a) 1539–1552.
[19] S.M. Richardson-Burns, J.L. Hendricks, D.C. Martin, Electrochemical polymerization of conducting polymers in living neural tissue, J. Neural Eng. 4 (2) (2007b) L6–L13.
[20] L. Ouyang, G.R., K.E. Feldman, D.C. Martin, Direct local polymerization of poly(3,4-ethylenedioxythiophene) in rat cortex, Prog. Brain Res. 194 (2011) 263–271.
[21] M.R. Abidian, D.C. Martin, Experimental and theoretical characterization of implantable neural microelectrodes modified with conducting polymer nanotubes, Biomaterials 29 (9) (2008) 1273–1283.

[22] M. Asplund, H. von Holst, O. Inganäs, Composite biomolecule/PEDOT materials for neural electrodes, Biointerphases 3 (3) (2008) 83–93.
[23] B. Paczosa, T. Blaz, J. Migdalski, A. Lewenstam, Conducting polymer films as model biological membranes. Electrochemical and ion-exchange properties of PPy and PEDOT films doped with heparin, Pol. J. Chem. 78 (9) (2004) 1543–1552.
[24] X.T. Cui, D.D. Zhou, Poly (3, 4-ethylenedioxythiophene) for chronic neural stimulation, IEEE Trans. Neural Syst. Rehabil. Eng. 15 (4) (2007) 502–508.
[25] R.A. Green, N.H. Lovell, G.G. Wallace, L.A. Poole-Warren, Conducting polymers for neural interfaces: challenges in developing an effective long-term implant, Biomaterials 29 (24–25) (2008) 3393–3399.
[26] L. Liu, J. Zhang, J. Zhao, F. Liu, Mechanical properties of graphene oxides, Nanoscale 4 (19) (2012) 5910–5916.
[27] D. Dechtrirat, B. Sookcharoenpinyo, P. Prajongtat, C. Sriprachuabwong, A. Sanguankiat, A. Tuantranont, S. Hannongbua, An electrochemical MIP sensor for selective detection of salbutamol based on a graphene/PEDOT:PSS modified screen printed carbon electrode, RSC Adv. 8 (1) (2018) 206–212.
[28] L.A. Mercante, M.H.M. Facure, R.C. Sanfelice, F.L. Migliorini, L.H.C. Mattoso, D.S. Correa, One-pot preparation of PEDOT:PSS-reduced graphene decorated with Au nanoparticles for enzymatic electrochemical sensing of H2O2, Appl. Surf. Sci. 407 (2017) 162–170.
[29] N. Muhammad, J. Abdullah, Y. Sulaiman, L.H. Ngee, Voltammetric determination of nitrophenol using PEDOT decorated graphene oxide as composite film, International Journal of Electrochemical Science 12 (10) (2017) 9432–9444.
[30] P. Pananon, C. Sriprachuabwong, A. Wisitsoraat, P. Chuysinuan, A. Tuantranont, P. Saparpakorn, D. Dechtrirat, A facile one-pot green synthesis of gold nanoparticle-graphene-PEDOT: PSS nanocomposite for selective electrochemical detection of dopamine, RSC Adv. 8 (23) (2018) 12724–12732.
[31] I.M. Taylor, E.M. Robbins, K.A. Catt, P.A. Cody, C.L. Happe, X.T. Cui, Enhanced dopamine detection sensitivity by PEDOT/graphene oxide coating on in vivo carbon fiber electrodes, Biosens. Bioelectron. 89 (2017) 400–410.
[32] L. Wang, H. Xu, Y. Song, J. Luo, W. Wei, S. Xu, X. Cai, Highly sensitive detection of quantal dopamine secretion from pheochromocytoma cells using neural microelectrode array electrodeposited with polypyrrole graphene, ACS Appl. Mater. Interfaces 7 (14) (2015) 7619–7626.
[33] M.H. Wang, B.W. Ji, X.W. Gu, H.C. Tian, X.Y. Kang, B. Yang, X.L. Wang, X. Chen, C.Y. Li, J.Q. Liu, Direct electrodeposition of Graphene enhanced conductive polymer on microelectrode for biosensing application, Biosens. Bioelectron. 99 (2018) 99–107.
[34] A. Wong, A.M. Santos, O. Fatibello, Determination of piroxicam and nimesulide using an electrochemical sensor based on reduced graphene oxide and PEDOT:PSS, J. Electroanal. Chem. 799 (2017) 547–555.
[35] G.Y. Xu, Z.A. Jarjesa, V. Desprez, P.A. Kilmartin, J. Travas-Sejdic, Sensitive, selective, disposable electrochemical dopamine sensor. based on PEDOT-modified laser scribed graphene, Biosens. Bioelectron. 107 (2018) 184–191.
[36] K. Catt, H. Li, V. Hoang, R. Beard, X.T. Cui, Self-powered therapeutic release from conducting polymer/graphene oxide films on magnesium, Nanomed. Nanotechnol. Biol. Med. 14 (7) (2017) 2495–2503.
[37] C.L. Weaver, J.M. LaRosa, X. Luo, X.T. Cui, Electrically controlled drug delivery from graphene oxide nanocomposite films, ACS Nano 8 (2) (2014) 1834–1843.
[38] C.T. Chen, T. Zhang, Q. Zhang, X. Chen, C.L. Zhu, Y.H. Xu, J.Z. Yang, J. Liu, D.P. Sun, Biointerface by cell growth on graphene oxide doped bacterial cellulose/poly(3,4-ethylenedioxythiophene) nanofibers, ACS Appl. Mater. Interfaces 8 (16) (2016) 10183–10192.
[39] W.B. Guo, X.D. Zhang, X. Yu, S. Wang, J.C. Qiu, W. Tang, L.L. Li, H. Liu, Z.L. Wang, Self-powered electrical stimulation for enhancing neural differentiation of mesenchymal stem cells on graphene-poly(3,4-ethylenedioxythiophene) hybrid microfibers, ACS Nano 10 (5) (2016) 5086–5095.
[40] Y.S. Hsiao, C.W. Kuo, P.L. Chen, Multifunctional graphene-PEDOT microelectrodes for on chip manipulation of human mesenchymal stem cells, Adv. Funct. Mater. 23 (37) (2013) 4649–4656.
[41] X. Luo, C.L. Weaver, S. Tan, X.T. Cui, Pure graphene oxide doped conducting polymer nanocomposite for bio-interfacing, J. Mater. Chem. B 1 (9) (2013) 1340–1348.
[42] C.L. Weaver, X.T. Cui, Directed neural stem cell differentiation with a functionalized graphene oxide nanocomposite, Adv. Healthc. Mater. 4 (9) (2015) 1408–1416.
[43] L. Yan, B.X. Zhao, X.H. Liu, X. Li, C. Zeng, H.Y. Shi, X.X. Xu, T. Lin, L.M. Dai, Y. Liu, Aligned nanofibers from polypyrrole/graphene as electrodes for regeneration of optic nerve via electrical stimulation, ACS Appl. Mater. Interfaces 8 (11) (2016) 6834–6840.
[44] A. Fabbro, D. Scaini, V.n. León, E. Vázquez, G. Cellot, G. Privitera, L. Lombardi, F. Torrisi, F. Tomarchio, F. Bonaccorso, Graphene-based interfaces do not alter target nerve cells, ACS Nano 10 (1) (2016) 615–623.
[45] M.M. Fan, C.L. Zhu, L. Liu, Q.L. Wu, Q.L. Hao, J.Z. Yang, D.P. Sun, Modified PEDOT by benign preparing N-doped reduced graphene oxide as potential bioelectrode coating material, Green Chem. 18 (6) (2016) 1731–1737.
[46] D. Kuzum, H. Takano, E. Shim, J.C. Reed, H. Juul, A.G. Richardson, J. de Vries, H. Bink, M.A. Dichter, T.H. Lucas, D.A. Coulter, E. Cubukcu, B. Litt, Transparent and flexible low noise graphene electrodes for simultaneous electrophysiology and neuroimaging, Nat. Commun. 5 (2014) 5259.
[47] D.W. Park, J.P. Ness, S.K. Brodnick, C. Esquibel, J. Novello, F. Atry, D.H. Baek, H. Kim, J. Bong, K.I. Swanson, A.J. Suminski, K.J. Otto, R. Pashaie, J.C. Williams, Z.Q. Ma, Electrical neural stimulation and simultaneous in vivo monitoring with transparent graphene electrode arrays implanted in GCaMP6f mice, ACS Nano 12 (1) (2018) 148–157.
[48] M. Ryu, J.H. Yang, Y. Ahn, M. Sim, K.H. Lee, K. Kim, T. Lee, S.J. Yoo, S.Y. Kim, C. Moon, M. Je, J.W. Choi, Y. Lee, J.E. Jang, Enhancement of interface characteristics of neural probe based on graphene, ZnO nanowires, and conducting polymer PEDOT, ACS Appl. Mater. Interfaces 9 (12) (2017) 10577–10586.
[49] H.-C. Tian, J.-Q. Liu, X.-Y. Kang, D.-X. Wei, C. Zhang, J.-C. Du, B. Yang, X. Chen, C.-S. Yang, Poly (3, 4-ethylenedioxythiophene)/graphene oxide composite coating for electrode-tissue interface, in: Engineering in Medicine and Biology Society (EMBC), 2014 36th Annual International Conference of the IEEE, IEEE, 2014a, pp. 1571–1574.
[50] H.-C. Tian, J.-Q. Liu, D.-X. Wei, X.-Y. Kang, C. Zhang, J.-C. Du, B. Yang, X. Chen, H.-Y. Zhu, Y.-N. NuLi, C.-S. Yang, Graphene oxide doped conducting polymer nanocomposite film for electrode-tissue interface, Biomaterials 35 (7) (2014b) 2120–2129.
[51] T.D.Y. Kozai, K. Catt, Z.H. Du, K. Na, O. Srivannavit, R.U.M. Haque, J. Seymour, K.D. Wise, E. Yoon, X.T. Cui, Chronic in vivo evaluation of PEDOT/CNT for stable neural recordings, IEEE Trans. Biomed. Eng. 63 (1) (2016) 111–119.
[52] N.A. Alba, Z.J. Du, K.A. Catt, T.D. Kozai, X.T. Cui, In vivo electrochemical analysis of a PEDOT/MWCNT neural electrode coating, Biosensors 5 (4) (2015) 618–646.
[53] C.L. Kolarcik, K. Catt, E. Rost, I.N. Albrecht, D. Bourbeau, Z. Du, T.D. Kozai, X. Luo, D.J. Weber, X.T. Cui, Evaluation of poly (3, 4-ethylenedioxythiophene)/carbon nanotube neural electrode coatings for stimulation in the dorsal root ganglion, J. Neural Eng. 12 (1) (2014), 016008.
[54] W.S. Hummers Jr., R.E. Offeman, Preparation of graphitic oxide, J. Am. Chem. Soc. 80 (6) (1958), 1339-1339.
[55] S. Yang, Rapid Neuronal Signaling Cascades Initiated by Corticosterone (Doctoral Dissertation, Lmu), 2012.
[56] M. Wall, Raman spectroscopy, Adv. Mater. Process. 170 (4) (2012) 35–38.
[57] R. Green, P. Matteucci, R. Hassarati, B. Giraud, C. Dodds, S. Chen, P. Byrnes-Preston, G. Suaning, L. Poole-Warren, N. Lovell, Performance of conducting polymer electrodes for stimulating neuroprosthetics, J. Neural Eng. 10 (1) (2013), 016009.
[58] S.J. Wilks, S.M. Richardson-Burn, J.L. Hendricks, D. Martin, K.J. Otto, Poly (3, 4-ethylene dioxythiophene)(PEDOT) as a micro-neural interface material for electrostimulation, Front. Neuroeng. 2 (2009) 7.
[59] S. Chen, W. Pei, Q. Gui, R. Tang, Y. Chen, S. Zhao, H. Wang, H. Chen, PEDOT/MWCNT composite film coated microelectrode arrays for neural interface improvement, Sensor Actuator Phys. 193 (2013) 141–148.
[60] D.R. Merrill, M. Bikson, J.G. Jefferys, Electrical stimulation of excitable tissue: design of efficacious and safe protocols, J. Neurosci. Methods 141 (2) (2005) 171–198.
[61] L. Aigner, S. Arber, J.P. Kapfhammer, T. Laux, C. Schneider, F. Botteri, H.-R. Brenner, P. Caroni, Overexpression of the neural growth-associated protein GAP-43 induces nerve sprouting in the adult nervous system of transgenic mice, Cell 83 (2) (1995) 269–278.
[62] S.M. Strittmatter, C. Fankhauser, P.L. Huang, H. Mashimo, M.C. Fishman, Neuronal pathfinding is abnormal in mice lacking the neuronal growth cone protein GAP-43, Cell 80 (3) (1995) 445–452.
[63] L.I. Benowitz, A. Routtenberg, GAP-43: an intrinsic determinant of neuronal development and plasticity, Trends Neurosci. 20 (2) (1997) 84–91.
[64] B.A. Yankner, L.I. Benowitz, L. Villa-Komaroff, R.L. Neve, Transfection of PC12 cells with the human GAP-43 gene: effects on neurite outgrowth and regeneration, Mol. Brain Res. 7 (1) (1990) 39–44.
[65] N. Li, X. Zhang, Q. Song, R. Su, Q. Zhang, T. Kong, L. Liu, G. Jin, M. Tang, G. Cheng, The promotion of neurite sprouting and outgrowth of mouse hippocampal cells in culture by graphene substrates, Biomaterials 32 (35) (2011) 9374–9382.
[66] B. Sun, T. Wu, J. Wang, D. Li, J. Wang, Q. Gao, M.A. Bhutto, H. El-Hamshary, S.S. Al-Deyab, X. Mo, Polypyrrole-coated poly (L-lactic acid-co-ε-caprolactone)/silk fibroin nanofibrous membranes promoting neural cell proliferation and differentiation with electrical stimulation, J. Mater. Chem. B 4 (41) (2016) 6670–6679.
[67] Q. Tu, L. Pang, L.L. Wang, Y.R. Zhang, R. Zhang, J.Y. Wang, Biomimetic choline-like graphene oxide composites for neurite sprouting and outgrowth, ACS Appl. Mater. Interfaces 5 (24) (2013) 13188–13197.
[68] F. Fiumara, S. Giovedì, A. Menegon, C. Milanese, D. Merlo, P.G. Montarolo, F. Valtorta, F. Benfenati, M. Ghirardi, Phosphorylation by cAMP-dependent protein kinase is essential for synapsin-induced enhancement of neurotransmitter release in invertebrate neurons, J. Cell Sci. 117 (21) (2004) 5145–5154.
[69] S. Hilfiker, V.A. Pieribone, A.J. Czernik, H.-T. Kao, G.J. Augustine, P. Greengard, Synapsins as regulators of neurotransmitter release, Phil. Trans. Biol. Sci. 354 (1381) (1999) 269–279.
[70] T.C. Südhof, The synaptic vesicle cycle, Annu. Rev. Neurosci. 27 (2004) 509–547.
[71] K.M. Turner, R.D. Burgoyne, A. Morgan, Protein phosphorylation and the regulation of synaptic membrane traffic, Trends Neurosci. 22 (10) (1999) 459–464.
[72] P. Danielsson, J. Bobacka, A. Ivaska, Electrochemical synthesis and characterization of poly (3, 4-ethylenedioxythiophene) in ionic liquids with bulky organic anions, J. Solid State Electrochem. 8 (10) (2004) 809–817.